A. Daşdemir

FORCED VIBRATIONS OF PRE-STRESSED SANDWICH PLATE-STRIP WITH ELASTIC LAYERS AND PIEZOELECTRIC CORE

Department of Mathematics, Faculty of Arts and Sciences, Kastamonu University, Kastamonu, Turkey; e-mail: ahmetdasdemir37@gmail.com

Abstract. Within the scope of the piecewise homogeneous body model with utilizing of the three dimensional linearized theory of electro-elastic waves in initially stressed bodies, a mathematical modeling the dynamical stress field problem occurred in a sandwich plate-strip is carried out. This plate consists of a piezoelectric core perfectly bonded to the elastic layers with initial stress under the action of a time-harmonic force resting on a rigid foundation. It is assumed that the piezoelectric material is poled perpendicular to free surface of the body. A governing system of the partial differential equations of motion is solved by employing the finite element method. The numerical results are presented illustrating the effect of certain dependencies of the problem on the propagations of the stresses and the electric displacements acting on the interface planes between the elastic layers and the piezoelectric core and between the plate-strip and the rigid foundation. In particular, an effect of the initial stress parameter and a change of the thickness of the piezoelectric core on the frequency response of the plate-strip is investigated.

Key words: piezoelectric core, finite element method, time-harmonic force, sandwich plate-strip.

1. Introduction.

Sandwich structures are a kind of composite materials consisting of three layers, i.e. a core layer is bonded to two layers. The core material may be selected more flexible or harder than the others. The use of composite sandwich structures in many engineering applications such as building construction, aerospace, nuclear and civil infrastructure has been increasing especially due to their features such as good energy, sound absorption ability and high flexural. Hence, the subject has been under the density study. The monographs [1] present detailed investigations on the subject.

Many researchers investigate many different problems based on various theories. Nayak et al. investigate the free vibration analysis of composite sandwich plates by using the family of new Reddy type elements based on Reddy's higher-order theory [2]. Chakraborti and Seikh study the buckling of sandwich plates with laminated stiff layers subjected to partial edge compression based on a refined higher order shear deformation theory [3]. Hazard and Bouillard consider the passive damping of structural vibrations by the use of viscoelastic layers [4]. Pandit et al. develop an improved plate model to study the buckling of laminated sandwich plate with transverly flexible core [5]. To analyze the static behavior of isotropic, sandwich and laminated plates, Xiang et al. present a new shear deformation theory [6]. Li et al. investigate the transient response of an orthotropic composite sandwich plate subjected to point-wise impulse loading with respect to a nonlinear high order core theory [7]. Tu et al. carve out a simple C^0 isoparametric finite element formulation based on the refined higher-order shear deformation theory for the bending and free vibration analysis of composite and sandwich laminate plates [8]. Hasheminejad and Gheshlaghi consider a three-

dimensional elasticity-based formulation for the dynamic response of an arbitrarily thick simply supported FGM rectangular plate under transient loads of arbitrary spatial and temporal variations resting on a Winkler – Pasternak elastic foundation [9]. Akbarov and Yahnioglu study a buckling delamination problem for a sandwich plate-strip with the piezoelectric face and elastic core layers which has two interface inner cracks by employing the finite element method [10]. Loja et al. develop the static and dynamic behavior of functionally graded sandwich structures with piezoelectric skins by B-spline finite strip models [11]. Shahraeeni et al. analyze analytically free and forced vibration of piezoelectric laminated plates coupled with rectangular acoustic cavities based on Kirchhoff plate model [12]. Sanker et al. present the dynamic instability behavior of sandwich panels with carbon nanotube (CNT) reinforced facesheets under the periodic load [13].

As far to the author's knowledge the forced vibration of a pre-stressed sandwich plate-strip with a piezoelectric core perfectly bonded to two elastic layers subjected to a time harmonic force resting on a rigid foundation has not been studied so far. To address the issue, the mathematical modeling of the problem under consideration is analytically solved by employing the finite element method. Most significant contributions of this work include the investigation of the effect of the different problem dependences on the frequency response of the considered sandwich plate-strip.

2. Statement of Problem.

Consider a sandwich plate-strip with length $2a$ and thickness h under the action of a time harmonic force resting on a rigid foundation as depicted in Fig. 1. It is consists of a piezoelectric core with the thickness h_2 bonded perfectly a two isotropic layer with the thickness h_1 and h_3 respectively. The poling direction of the piezoelectric material is assumed along the direction of the Ox_2 axis.

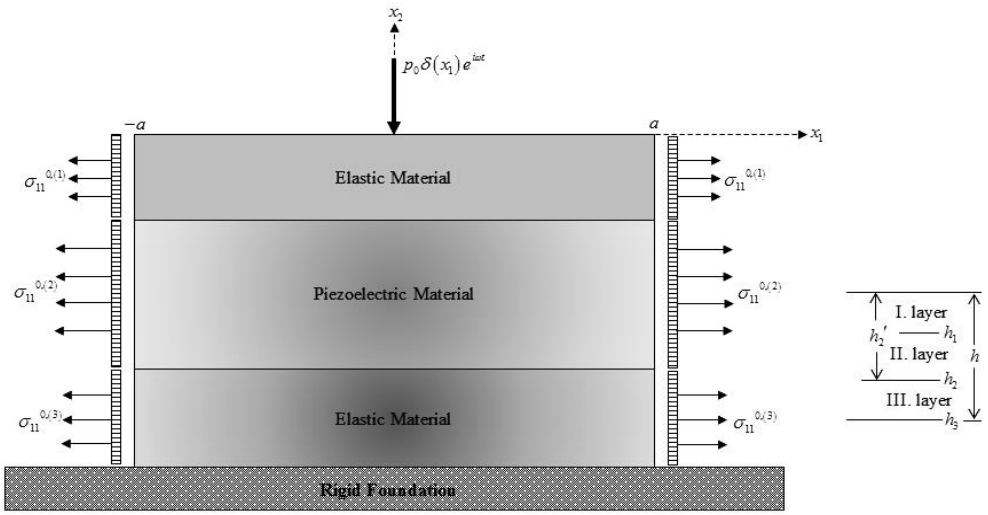

Fig. 1. Geometry of sandwich plate-strip with piezoelectric core.

The locations of the positions of the layers are determined by the Lagrangian coordinates, which in the natural state coincide with Cartesian coordinates. The values related to the upper, core and lower layers of plate-strip are denoted by the superscripts (1), (2) and (3), respectively, and the additional upper index 0 to the initial state. It is assumed that the length of plate-strip in the direction of the Ox_3 axis is infinite. However, since the force applied to the considered body extends to infinity in the direction of the Ox_3 axis, the plane deformation state appears on the Ox_1x_2 plane. All investigations are therefore made in the Ox_1x_2 plane. The plate-strip under consideration occupies the domain $B = B_1 \cup B_2 \cup B_3$, where

$$B_1 = \left\{ \left(x_1, x_2 \right) : -a \le x_1 \le a,\ -h_1 \le x_2 \le 0 \right\}; \tag{1}$$

$$B_2 = \left\{ \left(x_1, x_2 \right) : -a \le x_1 \le a,\ -h_2' \le x_2 \le -h_1 \right\}; \tag{2}$$

$$B_3 = \left\{ \left(x_1, x_2 \right) : -a \le x_1 \le a,\ -h \le x_2 \le -h_2' \right\}. \tag{3}$$

The general forms of the differential equations of motion for the small initial deformation can be expressed as follows [14 – 15]:

$$\sigma_{ij,j}^{(m)} + \left(\sigma_{kj}^{0,(m)} u_{i,k}^{(m)} \right)_{,j} = \rho^{(m)} \ddot{u}_i^{(m)}; \tag{4}$$

$$D_{i,i}^{(m)} + \left(D_j^{0,(m)} u_{i,j}^{m} \right)_{,i} = 0, \tag{5}$$

where $i,\ j,\ k = 1,\ 2$, $m = 1,2,3$, $\rho^{(m)}$ is the corresponding mass density in the natural state, $u_i^{(m)}$ and $D_i^{(m)}$ denote the mechanical and electrical displacements with respect to corresponding coordinate x_i, $\sigma_{ij}^{(m)}$ is the stress tensor, $\sigma_{kj}^{0,(m)}$ initial stress tensor and $D_j^{0,(m)}$ initial electrical displacement. The dot over the displacement components is time differentiation and the comma followed by the subscript i indicates the space-coordinate differentiation. Here and below, the repeated index in the subscript is summed with respect to that index. It should be noted that the equation in (4) is written for both the elastic phase and the piezoelectric phase. But the equation in (5) vanishes for the elastic phase since it concerns with the electrical displacements.

Before compounding each layer with one another and with rigid foundation, the layers are stretched or compressed separately in the direction Ox_1 by uniformly distributed normal forces. Hence, uniaxial homogenous initial stress state occurs in the plate-strip. This initial stress is determined by utilizing the linear theory of the electro-elasticity as

$$\sigma_{11}^{0,(m)} = q^{(m)},\ \sigma_{ij}^{0,(m)} = 0 \ \text{for all}\ ij \ne 11, \tag{6}$$

where $q^{(m)}$ is the known constant for each layer. According to all the foregoing assumptions and due to the character of piezoelectric material, an axial homogenous initial electric displacement emerges in the piezoelectric layer as

$$D_1^{0,(2)} = D_1^0 \ \text{and}\ D_2^{0,(2)} = D_2^0 = 0. \tag{7}$$

Note that initial stress and initial electric displacement cannot be the independent from each other. They must be self-consistent. This statement will be explained later.

The mechanical and geometrical relations for an isotropic elastic material and a piezoelectric material can respectively be written as

$$\sigma_{ij}^{(\ell)} = \lambda^{(\ell)} \varepsilon_{\theta\theta}^{(\ell)} \delta_{ij} + 2\mu^{(\ell)} \varepsilon_{ij}^{(\ell)}; \tag{8}$$

$$\sigma_{ij} = c_{ijkl} \varepsilon_{kl} - e_{kij} \varphi_{,k},\ D_i = e_{ikl} \varepsilon_{kl} - \gamma_{ik} \varphi_{,k}, \tag{9}$$

where $\ell = 1,\ 3$, $\lambda^{(m)}$ and $\mu^{(m)}$ are the Lamé constants for the elastic phase, c_{ijkl}, e_{kij} and γ_{ik} are mechanic, piezoelectric and dielectric constants, respectively for the piezoelectric phase, δ_{ij} is the Kronecker delta, φ is the electric potential, $\varepsilon_{ij}^{(m)}$ is the strain tensor and defined such that $\varepsilon_{ij}^{(m)} = \frac{1}{2}\left(u_{i,j}^{(m)} + u_{j,i}^{(m)} \right)$. Note that, since the piezoelectric material is only in the intermediate layer, the superscript is omitted.

Now the boundary and contact conditions are considered.

According to the foregoing discussions, on the free surface and on the ends of the plate-strip the following boundary conditions are described as

$$\sigma_{12}^{(1)}\Big|_{x_2=0} = 0,\ \sigma_{22}^{(1)}\Big|_{x_2=0} = -p_o\delta(x_1)e^{i\omega t}; \tag{10}$$

$$\left(q^{(m)}u_{\mathrm{j},1}^{(m)} + \sigma_{1j}^{(m)}\right)\Big|_{x_1=\mp a} = 0; \tag{11}$$

$$\left(D_1 + D_1^{0}u_{1,1}\right)\Big|_{\substack{x_1=\mp a \\ -h_2' < x_2 < -h_1}} = 0. \tag{12}$$

The surfaces of the piezoelectric layer are assumed to be mechanically free and electrically open. The boundary conditions can therefore be written as

$$\varphi\Big|_{\substack{x_1=\mp a \\ -h_2' < x_2 < -h_1}} = 0 \ \text{ and } \ \varphi\Big|_{\substack{x_2=-h_1,-h_2' \\ -a<x_1<-a}} = 0. \tag{13}$$

It is assumed that, on the interface planes between the layers of plate strip and between the plate-strip and rigid foundation, there exists the completely clamping state. In this case, the complete clamped conditions occur as

$$\sigma_{i2}^{(1)}\Big|_{x_2=-h_1} = \sigma_{i2}^{(2)}\Big|_{x_2=-h_1};\ \ \sigma_{i2}^{(2)}\Big|_{x_2=-h_2} = \sigma_{i2}^{(3)}\Big|_{x_2=-h_2}; \tag{14}$$

$$u_i^{(1)}\Big|_{x_2=-h_1} = u_i^{(2)}\Big|_{x_2=-h_1};\ \ u_i^{(2)}\Big|_{x_2=-h_2} = u_i^{(3)}\Big|_{x_2=-h_2}; \tag{15}$$

$$u_j^{(3)}\Big|_{x_2=-h} = 0. \tag{16}$$

With the above-mentioned, the formulation of the problem and the investigation of the governing field equations are thus exhausted.

3. FEM Modeling.

An analytical solution of the considered problem cannot be obtained; therefore, to solve this problem, the finite element method (FEM) is employed. Before starting solution, certain preparations are made. First of all, the dimensionless coordinate system is introduced as

$$\hat{x}_1 = \frac{x_1}{h};\ \ \hat{x}_2 = \frac{x_2}{h}. \tag{17}$$

In addition, recall the lineal load applied to the plate-strip is assumed to be time-harmonic, with frequency ω, as $p_o\delta(x_1)e^{i\omega t}$. Thus, all the corresponding dependent variables can be written in the form

$$\left\{\sigma_{ij}, u_i, \varepsilon_{ij}, D_i\right\}^{(m)}(x_1, x_2, t) = \left\{\overline{\sigma}_{ij}, \overline{u}_i, \overline{\varepsilon}_{ij}, \overline{D}_i\right\}^{(m)}(x_1, x_2)e^{i\omega t}, \tag{18}$$

where the superposed bar represents the amplitude of the corresponding quantities. After the coordinate transformation in (17) and substituting the expression in (18) into the foregoing equations and conditions, the same equations and boundary-contact conditions are obtained for the amplitude of the sought values by replacing the terms $\partial^2 u_j^{(m)}/\partial t^2$ and $p_o\delta(x_1)e^{i\omega t}$ with $-\omega^2 u_j^{(m)}$ and $p_o\delta(x_1)$, respectively.

To obtain FEM modeling of the last boundary-contact problem, the following functional is presented:

$$J\left(u^{(m)}\right) = \frac{1}{2}\sum_{m=1}^{3}\int_B\left[T_{ij}^{(m)}u_{j,i}^{(m)} + \rho^{(m)}\omega^2h^2\left\{\left(u_1^{(m)}\right)^2 + \left(u_2^{(m)}\right)^2\right\}\right]dB +$$

$$+\frac{1}{2}\int_{B_2} S_i\varphi_{,i}dB_2+\int_{-a/h}^{a/h}\frac{p_o\delta(x_1)}{\mu^{(1)}}u_2^{(1)}\Big|_{x_2=0}dx_1\,, \tag{19}$$

where

$$\begin{gathered}T_{ij}^{(m)}=\sigma_{ij}^{(m)}+\sigma_{in}^{0,(m)}u_{j,n}=w_{ijkn}u_{n,\mathrm{k}}^{(m)}+t_{ijk}\varphi_{,k};\\ S_i=D_i+D_n^{0}u_{i,n}=t_{kni}u_{n,k}+r_{ik}\varphi_{,k}.\end{gathered} \tag{20}$$

According to the constitutive equation in (9), the notations in (20) can clearly be written for the piezoelectric phase as

$$\begin{gathered}w_{1111}=c_{11}+q;\ \ w_{1122}=c_{13};\ \ w_{1212}=c_{44};\ \ w_{1221}=c_{44}+q;\\ w_{2112}=c_{44};\ \ w_{2121}=c_{44};\ \ w_{2211}=c_{13};\ \ w_{2222}=c_{33};\\ t_{111}=D_1^{0};\ t_{121}=e_{15};\ \ t_{211}=e_{15};\ \ t_{122}=D_1^{0};\\ t_{222}=e_{33};\ \ t_{112}=e_{31};\ \ r_{11}=-\gamma_{11};\ \ r_{22}=-\gamma_{33}.\end{gathered} \tag{21}$$

It is should be considered that, while $T_{ij}^{(m)}$ is computed, t_{1ii} is equal to zero. Note that the notations in (21) coincide with those for the elastic layers and $c_{11}=c_{33}=\lambda^{(\ell)}+2\mu^{(\ell)}$, $c_{13}=\lambda^{(\ell)}$, $c_{44}=\mu^{(\ell)}$, $q=q^{(\ell)}$, $e_{31}=e_{15}=e_{33}=0$ and $\gamma_{11}=\gamma_{33}=0$. In addition, all the components which do not insert into the relations in (21) are equal to zero. It is easily to confirm that

$$w_{ijkn}=w_{nkji}\,,\ t_{111}=t_{122}\ \text{ and }\ t_{ijk}=t_{jik}\,. \tag{22}$$

To show the validity of the functional presented in (19), Gauss's theorem is used. Taking the symmetry conditions in (22) into account,

$$\begin{gathered}\delta J\left(u^{(m)}\right)=\delta\left(\frac{1}{2}\sum_{m=1}^{3}\int_B\left[w_{ijkn}^{(m)}u_{n,k}^{(m)}u_{j,i}^{(m)}+t_{ijk}u_{j,i}^{(m)}\varphi_{,k}+\rho^{(m)}\omega^2h^2\left(u_1^{(m)}+u_2^{(m)}\right)^2\right]dB+\right.\\ \left.+\frac{1}{2}\int_{B_2}\left[t_{kni}u_{n,k}\varphi_{,i}+r_{ik}\varphi_{,k}\varphi_{,i}\right]dB_2+\int_{-a/h}^{a/h}\frac{p_o\delta(x_1)}{\mu^{(1)}}u_2^{(1)}\Big|_{x_2=0}dx_1\right)=\\ =\frac{1}{2}\sum_{m=1}^{3}\int_B\left[\left(w_{ijnk}^{(m)}+w_{knji}^{(m)}\right)u_{n,k}^{(m)}\delta u_{j,i}^{(m)}+\left(t_{ijk}+t_{jik}\right)\delta u_{j,i}\varphi_{,k}+2\rho^{(m)}\omega^2h^2u_j^{(m)}\delta u_j^{(m)}\right]dB+\\ +\int_{B_2}\left[t_{kni}u_{n,k}\delta\varphi_{,i}+r_{ik}\varphi_{,i}\delta\varphi_{,k}\right]dB_2+\int_{-a/h}^{a/h}\frac{p_o\delta(x_1)}{\mu^{(1)}}\delta u_2^{(1)}\Big|_{x_2=0}dx_1=\\ =\sum_{m=1}^{3}\int_B\left[w_{ijnk}^{(m)}u_{n,k}^{(m)}\delta u_{j,i}^{(m)}+t_{ijk}\delta u_{j,i}\varphi_k+\rho^{(m)}\omega^2h^2u_j^{(m)}\delta u_j^{(m)}\right]dB+\\ +\int_{B_2}\left[t_{kni}u_{n,k}\delta\varphi_i+r_{ik}\varphi_{,i}\delta\varphi_{,k}\right]dB_2+\int_{-a/h}^{a/h}\frac{p_o\delta(x_1)}{\mu^{(1)}}\delta u_2^{(1)}\Big|_{x_2=0}dx_1=\\ =\sum_{m=1}^{3}\int_S\left[w_{ijnk}^{(m)}u_{n,k}^{(m)}+t_{ijk}\varphi_{,k}\right]n_i\delta u_jdS+\int_{-a/h}^{a/h}\frac{p_o\delta(x_1)}{\mu^{(1)}}\delta u_2^{(1)}\Big|_{x_2=0}dx_1-\end{gathered} \tag{23}$$

$$-\sum_{m=1}^{3}\int_{B}\left[\left(w_{ijnk}{}^{(m)}u_{n,k}{}^{(m)}\right)_{,i}+\left(t_{ijk}\varphi_{,k}\right)_{,i}-\rho^{(m)}\omega^2h^2u_j{}^{(m)}\right]\delta u_j{}^{(m)}dB+$$

$$+\int_{B_2}\left[t_{kni}u_{n,k}+r_{ik}\varphi_{,i}\right]n_i\delta\varphi dS_2-\int_{B_2}\left[\left(t_{kni}u_{n,k}\right)_{,i}+\left(r_{ik}\varphi_i\right)_{,k}\right]\delta\varphi dB_2,$$

in which S_2 denotes the boundary of the domain B_2 and n_i is the components of $\boldsymbol{n}$, the outward unit vector normal to all the boundaries in the domain B.

Considering the statement

$$\delta J\left(\boldsymbol{u}^{(m)}\right)=0, \tag{24}$$

the equations of motion and the corresponding boundary-contact conditions given in (4)-(5) and (10) – (16) are obtained. So, the validity of the functional (19) suggested for the corresponding mathematical modeling is proven.

For the functional given in (19), the FEM modeling of the considered problem is created by the virtual work principle and the standard Rayleigh-Ritz method [17]. According to this approach, the domain B is divided into a finite element of sub-domains whose structures are four-node smooth rectangular elements. It is immediately specified that the number of the finite elements is determined from the desired numerical convergence requirement. According to the well-known procedure, after fairly extensive mathematical arrangements, a system of algebraic equations is obtained as

$$\left(\boldsymbol{K}-\omega^2\mathrm{M}\right)\tilde{\boldsymbol{u}}=\boldsymbol{F}, \tag{25}$$

where $\boldsymbol{K}$ is the stiffness matrix, M is the mass matrix, $\tilde{\boldsymbol{u}}$ is the column vector of unknown nodal displacements, and $\boldsymbol{F}$ is the force vector. To reduce the size of the present paper the explicit forms of the above-stated matrices and vectors are not given here. However, their explicit forms are directly derived from the equations (19) and (23) by using the considered procedure. So, with the above-stated the FEM modeling of the problem is exhausted.

4. Numerical Results.

Getting started with this section, certain remarks are made to more easily understand the numerical investigations. Certain notations are first introduced as

$$e=\frac{E^{(3)}}{E^{(1)}},\ \Omega^{(\ell)}=\omega h\sqrt{\frac{\rho^{(\ell)}}{\mu^{(\ell)}}}\ \text{and}\ \eta^{(\ell)}=\frac{q^{(\ell)}}{\mu^{(\ell)}} \tag{26}$$

for the elastic layers and

$$\Omega=\omega h\sqrt{\frac{\rho}{c_{44}}}\ \text{and}\ \eta=\frac{q}{c_{44}} \tag{27}$$

for the piezoelectric core. In the equations (26) and (27), $E^{(\ell)}$ is the Young modulus for the elastic layer, $\Omega^{(m)}$ is the dimensionless frequency parameter, and $\eta^{(m)}$ is the initial stress parameter.

Throughout the paper, all the numerical investigations are made at the interface planes between the upper elastic layer and the piezoelectric core (named “upper interface”), between the piezoelectric core and the lower elastic layer (named “lower interface” and between the plate-strip and rigid foundation (named “bottom surface”). Note that, when the corresponding parameters are equal, the superscript “(m)” will be omitted. It is assumed that, for all considered examples, the two elastic layers have the same thickness ($h_1=h_3$),

and the material $BaTiO_3$ is selected for the piezoelectric core. The following cases are also considered under $h/2a = 0,2$, $h_2/h = 0,5$, $\Omega = 0$ and $\eta = 0$ unless specified otherwise:

Case I: Aluminum (Upper layer) + $BaTiO_3$ (Core layer) + Steel (Lower layer)

Case II: $E^{(1)} = E^{(3)} = 1$, $\nu^{(1)} = \nu^{(3)} = 0,33$.

The electromechanical properties of materials considered are listed in Table. Changing values in any case under consideration will be specifically indicated.

Table. Values of material properties

Property	Elastic layer		Core Layer
	Aluminum	Steel	$BaTiO_3$
E (GPa)	70	210	-
ν	0,35	0,29	-
c_{11} (GPa)	-	-	150
c_{13} (GPa)	-	-	66
c_{33} (GPa)	-	-	146
c_{44} (GPa)	-	-	44
e_{31} (cm^{-2})	-	-	-4,35
e_{33} (cm^{-2})	-	-	17,5
e_{15} (cm^{-2})	-	-	11,4
γ_{11} (nFm^{-1})	-	-	11,15
γ_{33} (nFm^{-1})	-	-	12,6
ρ (kgm^{-3})	2712	7850	7280

As previously mentioned, the self-consistent condition of the initial stress (stretching or compressing) field for the piezoelectric phase should be satisfied. In this study, a case such that only a uniformly distributed normal initial stress field is considered. Then considering the constitutive equations, the equation $D_1^0 = q^{(2)}\left(c_{13}e_{33} - c_{33}e_{31}\right)/\left(c_{13}^{\ 2} - c_{11}c_{33}\right)$ can directly be derived for the piezoelectric phase. The values of the initial stress parameter $\eta^{(m)}$ are chosen at asymmetric interval – 0,07 to 0,07.

Before starting to present numerical results, the validity of the numerical algorithms and programs composed by the author under consideration must be verified. To do this, certain special cases are considered, and it will be shown that the obtained numerical results converge to the previous ones and the findings agree well with the foregoing discussion.

In Fig. 2, the distribution of the normal stress $\sigma_{22}h/p_0$ with respect to the line x_1/h on the bottom surface for Case II and $h_2 << h$ is displayed. This figure gives the opportunity to compare the numerical results obtained by using the present FEM algorithm with the ones given by Uflyand [18] for the plate with infinite length. Note that the starred graph in Fig. 2 means the one in [18]. The geometry of the considered body begins to resemble a semi-infinite structure as $h/2a \to 0$. In this case, the present numerical results must converge to the corresponding ones obtained in Ref. [18] as $h/2a \to 0$. This statement is demonstrated by the graphs in Fig. 2 plotted on the bottom surface.

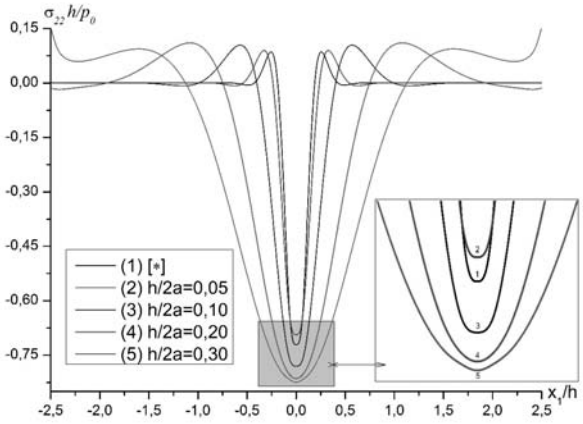

Fig. 2. The variation of $\sigma_{22}h / p_0$ versus the line x_1 / h for different thickness ratios under Case II on the bottom surface.

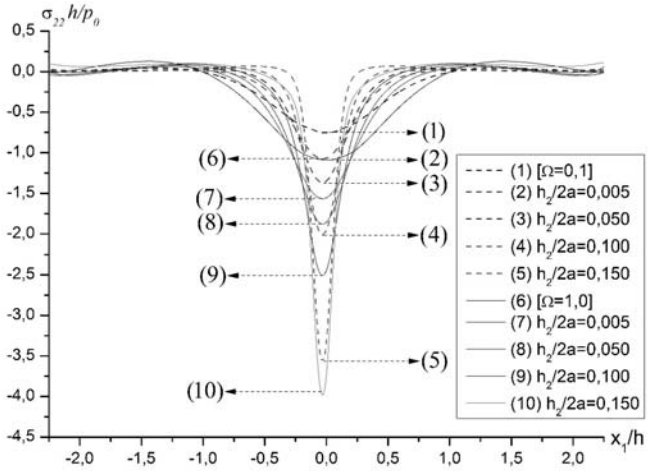

Fig. 3, a. The variation **of** $\sigma_{22}h / p_0$ versus the line x_1 / h for different piezoelectric thickness ratios under Case I at the upper interface.

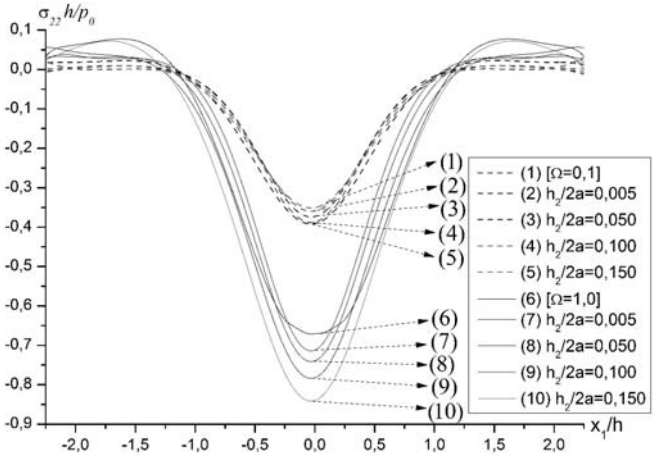

Fig. 3, b The variation of $\sigma_{22}h / p_0$ versus the line x_1 / h for different piezoelectric thickness ratios under Case I on the bottom surface.

Fig. 3 shows the distribution of the normal stress $\sigma_{22}h/p_0$ with respect to the line x_1/h for various thicknesses of the piezoelectric core under Case I at the upper interface and on the bottom surface. Note that the notation $[\Omega = \bullet]$ means the corresponding one in Ref. [16], and the solid (dashed) line graphs are plotted for $\Omega = 0,1$ $(\Omega = 1,0)$. The geometry of the plate-strip begins to resemble that in Ref [16] as $h_2 \to 0$. It can easily be observed from the graphs in Fig. 3 that the numerical results converge to the corresponding ones given in Ref. (16) for both interface and bottom surface under the condition $h_2 \to 0$.

Now, the effect of the ratio of the Young modulus of the elastic layers on $\sigma_{22}h/p_0$ and D_2h/p_0 along the line x_1/h is given in Fig. 4 under Case II, $h_2/h = 0,75$ and $\Omega = 0,3$. According to the well-known mechanical consideration, an increase in the values of the ratio e must give rise to a decrease in the absolute values of $\sigma_{22}h/p_0$ for the multi-layered body. Indeed, this prediction is clearly observed from the graphs in Fig. 4. In addition, it can be said that there exist certain locations where the values of $\sigma_{22}h/p_0$ and D_2h/p_0 are independent of the ratio e.

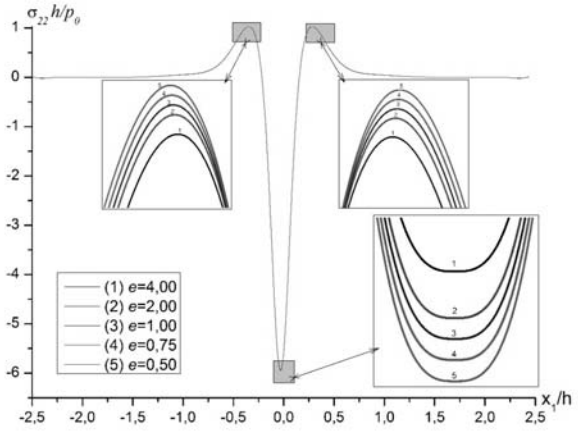

Fig. 4, a. The variation of $\sigma_{22}h/p_0$ versus the line x_1/h for various e under Case II and $\Omega = 0,3$ at the upper interface.

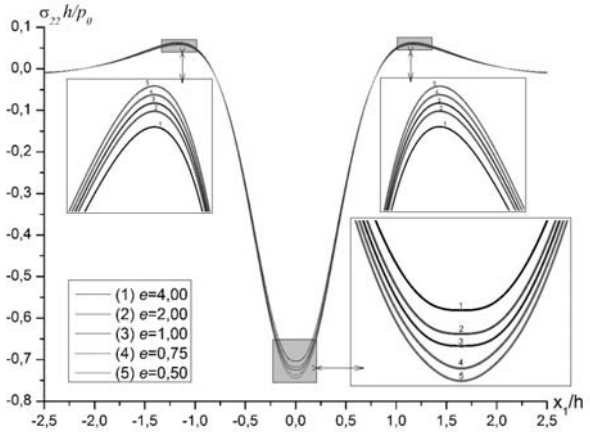

Fig. 4, b The variation of $\sigma_{22}h/p_0$ versus the line x_1/h for various e under Case II and $\Omega = 0,3$ at the lower interface.

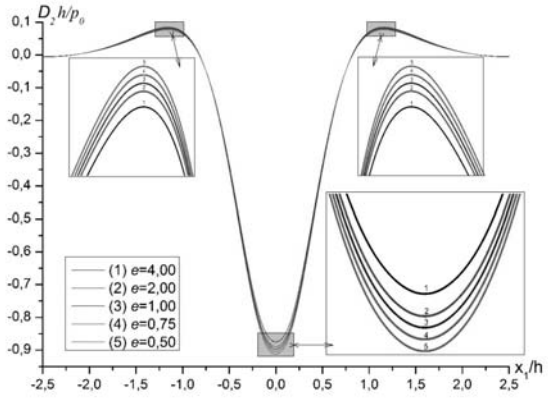

Fig. 4, c .The variation of D_2h/p_0 versus the line x_1/h for various e under Case II and $\Omega = 0,3$ at the lower interface.

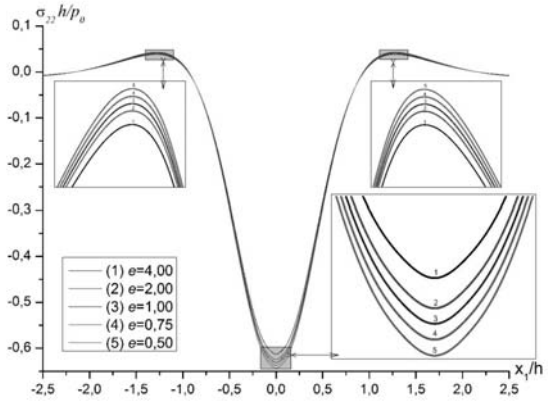

Fig. 4, d. The variation of $\sigma_{22}h/p_0$ versus the line x_1/h for various e under Case II and $\Omega = 0,3$ on the bottom surface.

The numerical results obtained from Figs. 2 and 3 show that, under certain special cases, the distributions of the stress $\sigma_{22}h/p_0$ converge to the previous ones. Besides, the findings in Fig. 4 agree well with the well-known foregoing mechanical considerations. In this way, the validity and trustiness of the algorithm and programs has been shown.

In Fig. 5, the effect of the initial stretching (compressing) η on the distribution of $\sigma_{22}h/p_0$ and D_2h/p_0 with respect to the line x_1/h under Case I, $h_2/h = 0,75$ and $\Omega = 0,3$ at the upper and lower interfaces and on the bottom surface is displayed. It can be shown from the graphs in Fig. 5 that, under $-x_1^*/h < x_1/h < x_1^*/h$ the absolute values of $\sigma_{22}h/p_0$ and D_2h/p_0 decrease (increase) with increasing the initial stretching (compressing) parameter. But under $-x_1^{**}/h < x_1/h < -x_1^*/h$ and $x_1^*/h < x_1/h < x_1^{**}/h$, the absolute values of $\sigma_{22}h/p_0$ and D_2h/p_0 decrease with (increasing) the initial stretching (compressing) parameter. Note that the values of x_1^*/h and x_1^{**}/h can be observed in Fig. 5 and are different at the upper and lower interfaces and on the bottom surface. As can be seen from Fig. 5, the effect of the initial stretching parameter applied to the body on $\sigma_{22}h/p_0$ and D_2h/p_0 is the opposite of that for the initial compressing parameter.

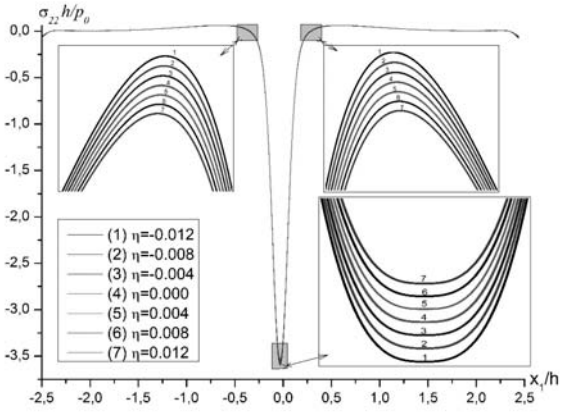

Fig. 5, a. The variation of $\sigma_{22}h/p_0$ versus the line x_1/h for various η under Case I and $\Omega = 0,3$ at the upper interface.

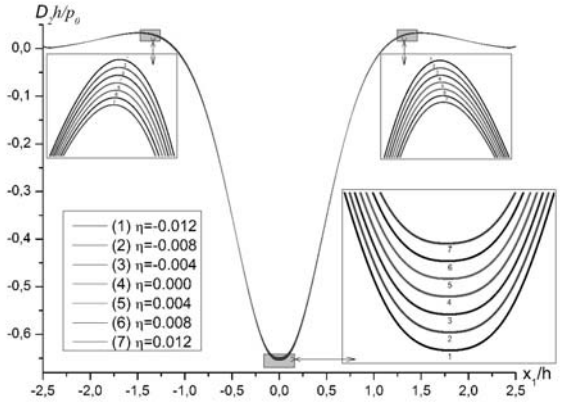

Fig. 5, b. The variation of D_2h/p_0 versus the line x_1/h for various η under Case I and $\Omega = 0,3$ at the lower interface.

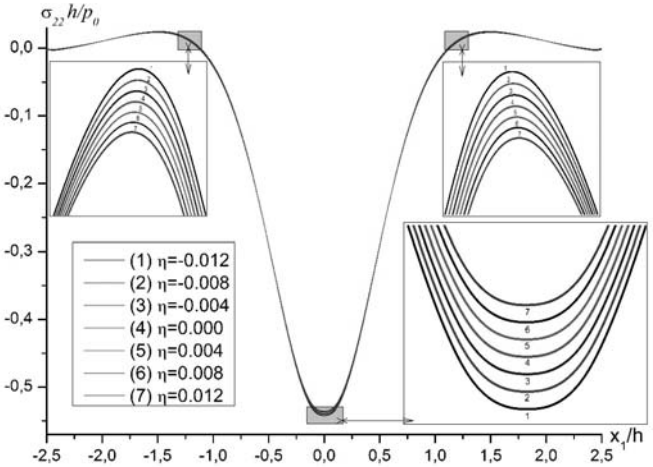

Fig. 5, c. The variation of $\sigma_{22}h/p_0$ versus the line x_1/h for various η under Case I and $\Omega = 0,3$ at the lower interface.

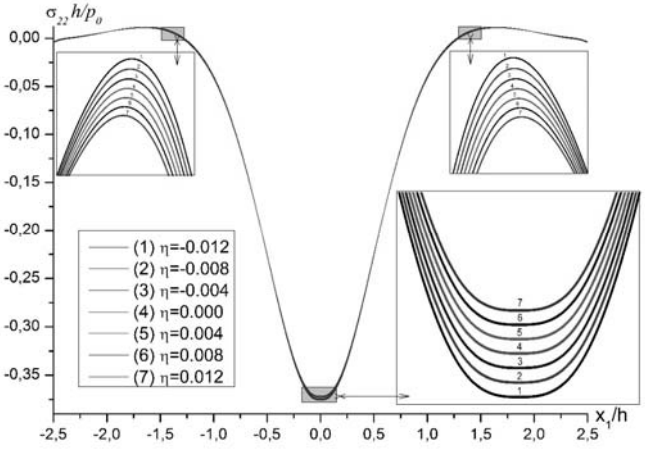

Fig. 5, d. The variation of $\sigma_{22}h/p_0$ versus the line x_1/h for various η under Case I and $\Omega = 0,3$ on the bottom surface.

To observe an influence of a change in values of the thickness of the piezoelectric core on this effect, Fig. 6 is now considered, which displays the variations of $\sigma_{22}h/p_0$ and D_2h/p_0 with respect to the initial stress parameter η at the points $(0,-h_1/h)$, $(0,-h_2/h)$ and $(0,-1)$ under the same assumptions in Fig. 5. Both the stress $\sigma_{22}h/p_0$ and the electrical displacement D_2h/p_0 depend linearly on the initial stress parameter. It can be shown that the slope of this linear dependence increases towards to the bottom surface. The type of material used in each layer causes to this result. By the same token, the slope of each graph decrease with increasing the thickness of the core layer. It can be said from this result that, when the thickness of the piezoelectric core decreases, the effect of both the initial stretching and initial compressing on σ_{22} and D_2 increases.

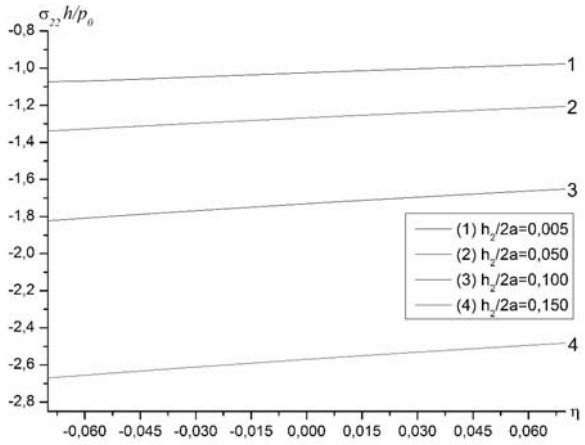

Fig. 6, a. The dependencies between $\sigma_{22}h/p_0$ and η for various $h_2/2a$ under Case I and $\Omega = 0,3$ at the point $(0,-h_1/h)$.

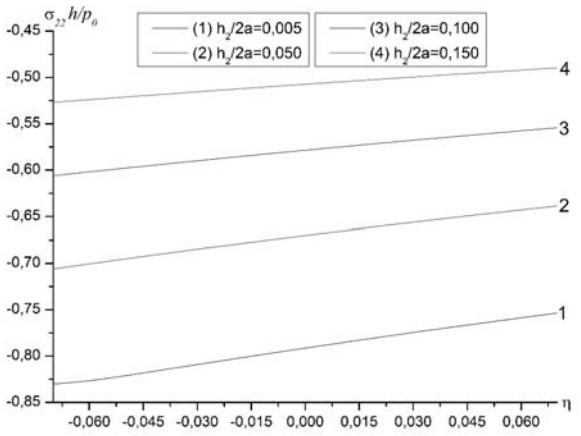

Fig. 6, b. The dependencies between $\sigma_{22}h/p_0$ and η for various $h_2/2a$ under Case I and $\Omega = 0,3$ at the point $(0,-h_2/h)$.

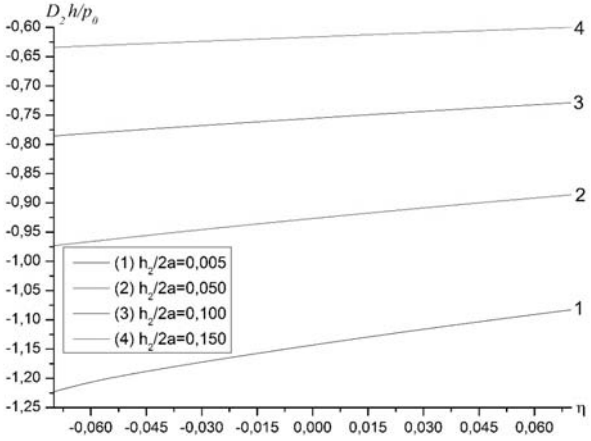

Fig. 6, c. The dependencies between D_2h/p_0 and η for various $h_2/2a$ under Case I and $\Omega = 0,3$ at the point $(0,-h_2/h)$.

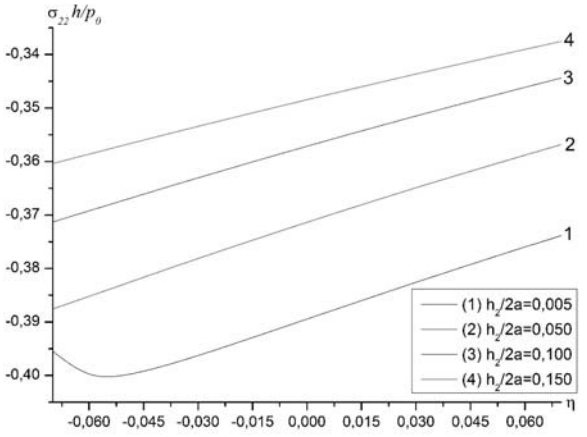

Fig. 6, d. The dependencies between $\sigma_{22}h/p_0$ and η for various $h_2/2a$ under Case I and $\Omega = 0,3$ at the point $(0,-1)$.

The numerical results obtained have been presented for the constant values of Ω until now. But the one of the main aims of the present paper is to investigate certain problem parameters on the frequency response of the stress $\sigma_{22}h/p_0$ and the electrical displacement D_2h/p_0. Thereafter, the influence of the relevant parameters on the frequency response of $\sigma_{22}h/p_0$ and D_2h/p_0 will be analyzed at the points $(0,-h_1/h)$, $(0,-h_2/h)$ and $(0,-1)$ under Case I unless otherwise.

Fig. 7 presents the variation of the stress $\sigma_{22}h/p_0$ and the electrical displacement D_2h/p_0 with the dimensionless frequency Ω for various thickness h_2. As can be seen from the graphs in this figure, the absolute values of $\sigma_{22}h/p_0$ and D_2h/p_0 decrease with the dimensionless frequency Ω. Also, while the absolute values of $\sigma_{22}h/p_0$ decrease with the thickness h_2 at $(0,-h_1/h)$, the absolute values of $\sigma_{22}h/p_0$ and D_2h/p_0 decrease with increasing the thickness h_2 at the other points.

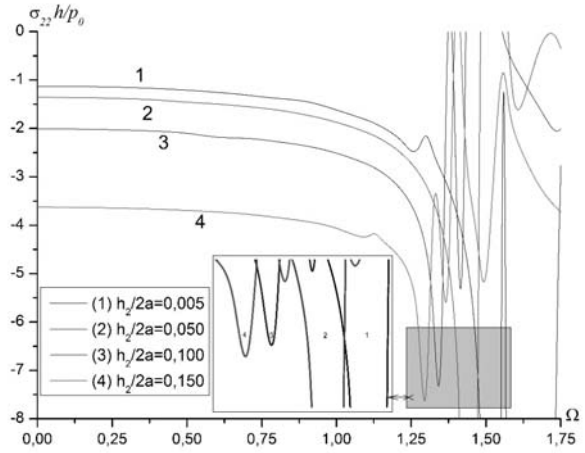

Fig. 7, a. The dependencies between $\sigma_{22}h/p_0$ and Ω for various $h_2/2a$ under Case I at the point $(0,-h_1/h)$.

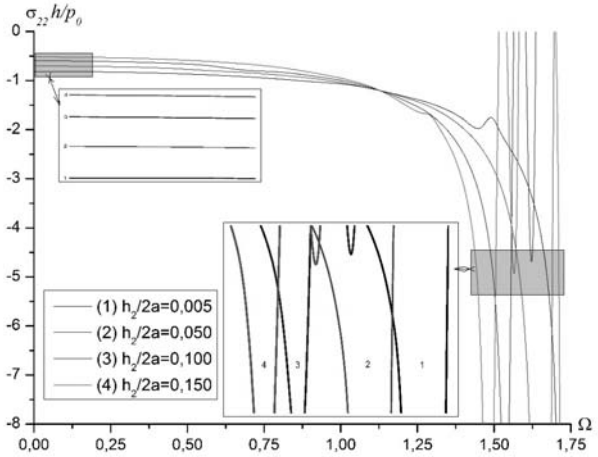

Fig. 7, b. The dependencies between $\sigma_{22}h/p_0$ and Ω for various $h_2/2a$ under Case I at the point $(0,-h_2/h)$.

This difference in Fig. 7, *a* is a natural result of its proximity to free surface of the investigated point. It follows from the investigations of the graphs that there exist locations where $\sigma_{22}h/p_0$ and D_2h/p_0 reach the extrema for the certain values of Ω. These values are called as its "resonance" values and denoted $\Omega_*^{(m)}$. The graphs show that the resonance values of Ω decrease with increasing the thickness h_2. Moreover, the numerical results prove that the "resonance" values of Ω depend on the selected material and on the material type. For instance, the resonance values of Ω for elastic layers are significantly smaller than that for the piezoelectric core. Clearly, $\Omega_*^{(Al)} < \Omega_*^{(St)} < \Omega_*^{(BaTiO_3)}$. An increase in the values of the thickness h_2 causes to increase the number of the local extremums of σ_{22} with respect to Ω. The dependences between $\sigma_{22}h/p_0$ and Ω and between D_2h/p_0 and Ω are non-monotonic. This result agrees well with the previous mechanical consideration. In addition, for $\Omega > 1,2$, the oscillating characters of $\sigma_{22}h/p_0$ and D_2h/p_0 become more sensitive for the present system. It follows from the foregoing investigations that the obtained results coincide with the ones in Ref. [16]. Thus, the validity and trustiness of the PC program composed by the author is confirmed again.

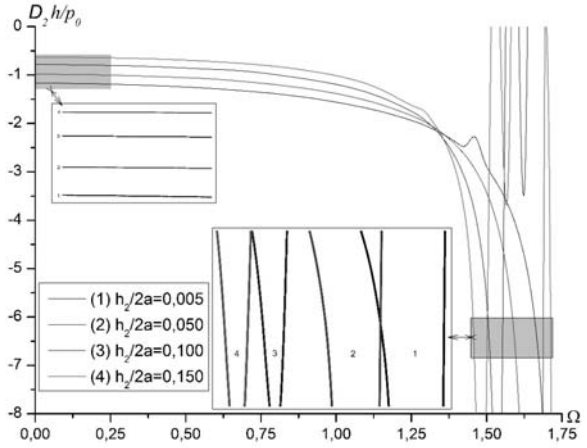

Fig. 7, c. The dependencies between D_2h/p_0 and Ω for various $h_2/2a$ under Case I at the point $(0,-h_2/h)$.

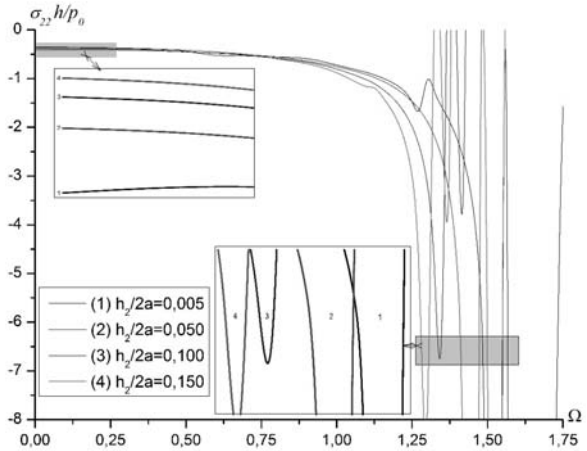

Fig. 7, d. The dependencies between $\sigma_{22}h/p_0$ and Ω for various $h_2/2a$ under Case I at the point $(0,-1)$.

It can be shown from the above discussions that the oscillating character of the distribution of $\sigma_{22}h/p_0$ is to be similar to that for D_2h/p_0 (in the qualitative sense). Thereafter, to reduce the size of the paper, so all the numerical investigations are only made at the points $(0,-h_2/h)$ and $(0,-1)$ for the normal stress $\sigma_{22}h/p_0$.

The numerical results given in Fig. 8 allow to obtain certain conclusions on the influence of a changes of the ratio $h/2a$ on the frequency response of the sandwich plate- strip. According to the graphs in Fig. 8, an increase in the values of $h/2a$ causes to decrease of the numbers of the local maximums and minimums of $\sigma_{22}h/p_0$ with respect to the dimensionless frequency Ω. The values of $\Omega_*^{(m)}$ decrease with increasing the ratio $h/2a$. While the values of the ratio $h/2a$ decrease, the oscillating character of the distribution of $\sigma_{22}h/p_0$ becomes more sensitive.

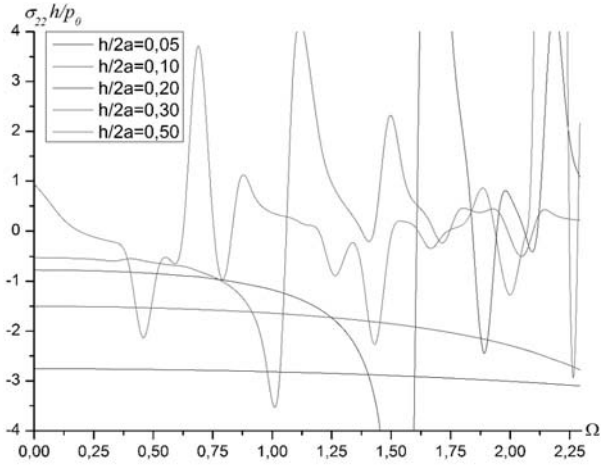

Fig. 8, a. The dependencies between $\sigma_{22}h/p_0$ and Ω for various $h/2a$ under Case I at the point $(0,-h_2/h)$.

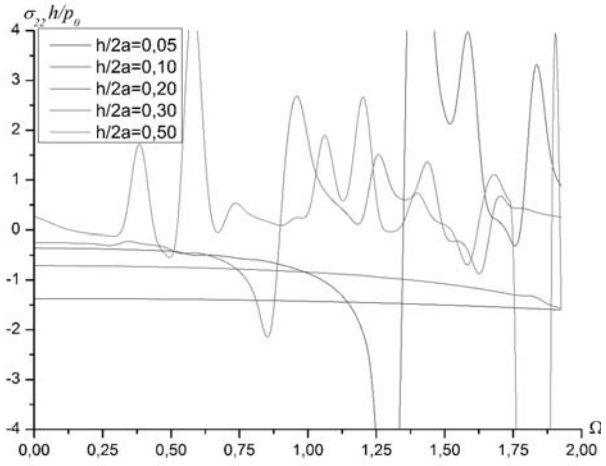

*Fig. 8, b***.** The dependencies between $\sigma_{22}h/p_0$ and Ω for various $h/2a$ under Case I at the point $(0,-1)$.

To investigate the effect of the initial stretching and compressing parameters on the distribution of $\sigma_{22}h/p_0$ with respect to the dimensionless frequency Ω, Fig. 9 is now considered. It follows from the graphs in Fig. 9 that the influence of the initial stretching and compressing parameters on the frequency response of the stress $\sigma_{22}h/p_0$ is significantly not only in the quantitative sense but also in the qualitative sense. Moreover, it can be shown that there exist certain locations where the parametric resonance of $\sigma_{22}h/p_0$ occurs for some values of the parameter η. An increase in the values of the initial stretching (compressing) parameter η causes to increase (decrease) the values of $\Omega_*^{(m)}$. Under the medium without the initial stress, i.e. $\eta = 0$, the resonance of the current system occur on the point where $\Omega \approx 1,2$. The initial stretching prevents the resonance value of $\sigma_{22}h/p_0$, but the initial compressing exceeds the corresponding resonance value.

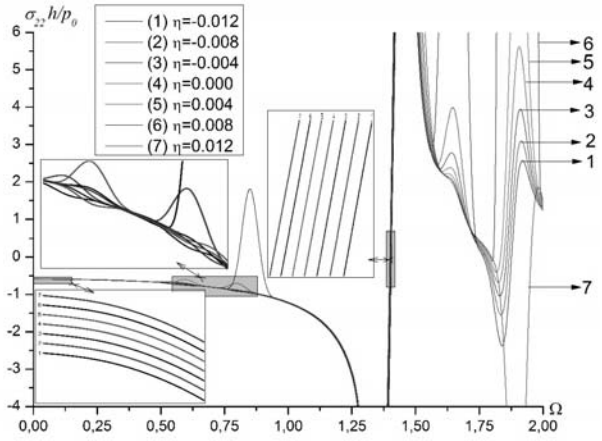

Fig. 9, а. The dependencies between $\sigma_{22}h/p_0$ and Ω for various η under Case I at the point $(0,-h_2/h)$.

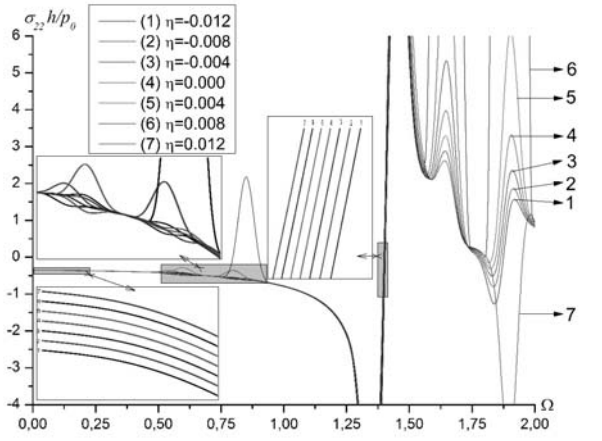

Fig. 9, б. The dependencies between $\sigma_{22}h/p_0$ and Ω for various η under Case I at the point $(0,-h_2/h)$.

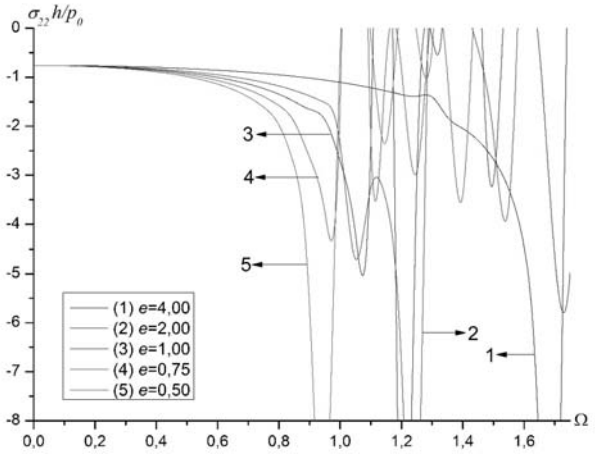

Fig. 10, a. The dependencies between $\sigma_{22}h/p_0$ and Ω for various e under Case I at the point $(0,-h_2/h)$.

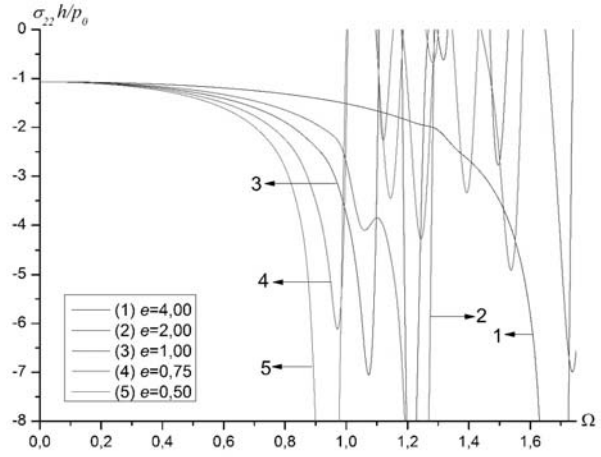

Fig. 10, b. The dependencies between $\sigma_{22}h/p_0$ and Ω for various e under Case I at the point $(0,-1)$.

Fig. 10 displays the effect of the parameter e on the variation of $\sigma_{22}h/p_0$ with respect to the dimensionless frequency Ω under Case II. The numerical results observed in Fig. 10 indicate that the values of $\Omega_*^{(m)}$ decrease with the parameter e. An increase in the values of the parameter e causes to decrease the numbers of the local maximums and minimums of $\sigma_{22}h/p_0$ with respect to Ω. Moreover, when the values of Ω decrease, the effect of the parameter e on the variation of $\sigma_{22}h/p_0$ damps rapidly. The resonance values at the lower interface are less than those on the bottom surface.

5. Conclusion.

In the present paper, the forced vibration problem for a pre-stressed sandwich plate-strip with a piezoelectric core perfectly bonded to two elastic layers under the action of a time-harmonic force on the rigid foundation is investigated within the scope of the exact equations of electro-elasticity in framework of the piecewise homogeneous body model. The

considered problem is numerically solved by employing the finite element method. The effect of various problem parameters on the frequency response of the sandwich plate-strip is examined. According to all the numerical investigations, certain inferences of the important results can be drawn as follows:

the effect of the initial stretching on the corresponding stress and electrical displacement components is opposite of that of the initial compressing;

an increase in the thickness of the piezoelectric core causes to increase the number of the local extremums of σ_{22} with respect to Ω;

the resonance values of the piezoelectric material are smaller than those of the elastic materials;

by increasing the length of the plate-strip for fixed thickness of that, or by decreasing the thickness of the plate for fixed length of that the numbers of the local extremums of σ_{22} decrease;

by decreasing the ratio of Young modulus of the elastic layers, the resonance values of the current system decrease;

while the initial stretching prevents the resonance value of the external force, the initial compressing exceeds this resonance value.

The numerical results listed above have been presented under two different cases, but note that they also have a general validity in a qualitative sense. Moreover, these numerical results are encountered daily in the engineering practice under an impact treatment of metals which lie on the others.

6. Acknowledgements.

The author is a member of the research project supported by Research Fund of Kastamonu University under project number KÜ-BAP01/2015-3.

Р Е З Ю М Е . В рамках моделі кусково-однорідного тіла з використанням тривимірної теорії електропружних хвиль в початково напружених тілах проведено математичне моделювання задачі про поле динамічних напружень, що виникає в шаруватій плиті-полосі. Ця плита складається з п'єзоелектричного ядра, яке граничить з пружним шарами з початковими напруженнями, і перебуває на абсолютно твердій основі. Приймається, що п'єзопружний матеріал поляризований перпендикулярно до вільної поверхні пластини. Основна система диференціальних рівнянь з частинними похідними розв'язана методом скінченних елементів. Представлено числові результати, які ілюструють вплив певних залежностей задачі про поширення напружень і електричних зміщень, які діють на площинах розділу пружних шарів і п'єзоелектричного ядра та плитою і абсолютно твердою основою. Зокрема, вивчено вплив параметра початкового напруження і зміни товщини п'єзопружного ядра на частотні характеристики плити-стержня.

1. *Vinson J.R.* Plate and Panel Structures of Isotropic, Composite and Piezoelectric Materials, Including Sandwich Construction. – Dordrecht: Springer, 2005. – 424 p.
2. *Nayak A.K., Moy S.S.J., Shenoi R.A.* Free vibration analysis of composite sandwich plates based on Reddy's higher-order theory // Composites Part B. – 2002. – **33** (7). – P. 505 – 519.
3. *Chakrabarti A., Sheikh A.H*. Buckling of laminated sandwich plates subjected to partial edge compression // Int. J. Mech. Sci. – 2005. – **47**(3). – P. 418 – 436.
4. *Hazard L., Bouillard P*. Structural dynamics of viscoelastic sandwich plates by the partition of unity finite element method // Comput. Method Appl. M. – 2007. – **196**. – P. 4101 – 4116.
5. *Pandit M.K., Singh B.N., Sheikh A.H*. Buckling of laminated sandwich plates with soft core based on an improved higher order zigzag theory // Thin. Wall. Struct. – 2008. – **46** (11). – P. 1183 – 1191.
6. *Xiang S. Wang K., Ai Y., Sha Y., Shi H.* Analysis of isotropic, sandwich and laminated plates by a meshless method and various shear deformation theories // Compos. Struct. – 2009. – **91** (1). – P. 31 – 37.

7. *Li R., Kardomateas G.A., Simitses G.J.* Point-wise impulse (blast) response of a composite sandwich plate including core compressibility effects // Int. J. Solids. Struct. – 2009. – **46**(10). – P. 2216 – 2223.
8. *Tu T.M., Thach L.N., Quoc T.H.* Finite element modeling for bending and vibration analysis of laminated and sandwich composite plates based on higher-order theory // Comp. Mater. Sci. – 2010. – **49** (4). – P. S390 – S394.
9**.** *Hasheminejad S.M., Gheshlaghi B.* Three-dimensional elastodynamic solution for an arbitrary thick FGM rectangular plate resting on a two parameter viscoelastic foundation // Compos. Struct. – 2012. – **94** (9). – P. 2746 – 2755.
10. *Akbarov S.D., Yahnioglu N.* Buckling delamination of a sandwich plate-strip with piezoelectric face and elastic core layers // Appl. Math. Model. – 2013. – **37**. – P. 8029 – 8038.
11. *Loja M.A.R., Soares, C.M.M., Barbosa, J.I.* Analysis of functionally graded sandwich plate structures with piezoelectric skins using B-spline finite strip method // Compos. Struct. – 2013. – **96.** – P. 606 – 615.
12. *Shahraeeni M., Shakeri R., Hasheminejad S.M.* An analytical solution for free and forced vibration of a piezoelectric laminated plate coupled with an acoustic enclosure // Comput. Math. Appl. – 2015. – **69** (11). – P. 1329 – 1341.
13. *Sankar A., Natarajan S. Ganapathi M*. Dynamic instability analysis of sandwich plates with CNT reinforced facesheets // Compos. Struct. – 2016. – **146** (20). – P. 187 – 200.
14. *Guz A.N.* Elastic Waves in a Body with Initial (Residual) Stresses. – Kiev: «A.C.K.», 2004. –672 p.
15. *Yang J.* An Introduction to the Theory of Piezoelectricity. – USA, New York: Springer, 2005. – 300 p.
16**.** *Daşdemir A., Eröz M.* Mathematical Modeling of dynamical stress field problem for a pre-stressed bi-layered plate-strip // Bull. Malays. Math. Sci. Soc. – 2015. – **38** (2). – P. 733 – 760.
17. *Zienkiewicz O.C., Taylor R.L.* The Finite Element Method. Vol.1. Basic Formulation and Linear Problems. – London: McGraw-Hill, 1989. – 648 p.
18. *Uflyand Y.S*. Integral Transformations in the Theory of Elasticity. – Moskow – Leningrad: USSR Academy of Science, 1963. – 367 p.

From the Editorial Board: The article corresponds completely to submitted manuscript.

Поступила 15.12.2016 Утверждена в печать 30.01.2018